

# Experimental test of Sinai's model in DNA unzipping

Cathelijne ter Burg<sup>1</sup>, Paolo Rissone<sup>2</sup>, Marc Rico-Pasto<sup>2</sup>, Felix Ritort<sup>2,3</sup> and Kay Jörg Wiese<sup>1</sup>  
<sup>1</sup>Laboratoire de Physique de l'École Normale Supérieure, ENS, Université PSL, CNRS, Sorbonne Université,  
 Université Paris-Diderot, Sorbonne Paris Cité, 24 rue Lhomond, 75005 Paris, France.

<sup>2</sup>Small Biosystems Lab, Condensed Matter Physics Department, Universitat de Barcelona,  
 Carrer de Martí i Franquès 1, 08028 Barcelona, Spain.

<sup>3</sup>Institut de Nanociència i Nanotecnologia (IN2UB), Universitat de Barcelona, 08028 Barcelona, Spain

The experimental measurement of correlation functions and critical exponents in disordered systems is key to testing renormalization group (RG) predictions. We mechanically unzip single DNA hairpins with optical tweezers, an experimental realization of the diffusive motion of a particle in a one-dimensional random force field, known as the *Sinai model*. We measure the unzipping forces  $F_w$  as a function of the trap position  $w$  in equilibrium and calculate the force-force correlator  $\Delta_m(w)$ , its amplitude, and correlation length, finding agreement with theoretical predictions. We study the universal scaling properties since the effective trap stiffness  $m^2$  decreases upon unzipping. Fluctuations of the position of the base pair at the unzipping junction  $u$  scales as  $u \sim m^{-\zeta}$ , with a *roughness exponent*  $\zeta = 1.34 \pm 0.06$ , in agreement with the analytical prediction  $\zeta = \frac{4}{3}$ . Our study provides a single-molecule test of the functional RG approach for disordered elastic systems in equilibrium.

**Introduction.** Heterogeneity and disorder pervade physical and biological matter [1–3]. Since Schrödinger's conception of the gene as an a-periodic crystal [4], disorder is recognised as a crucial ingredient for life [5]. The readout of the genetic information encoded in DNA can be modeled with polymers in random potentials, such as Sinai's model [6]. The latter describes the dynamics of a particle diffusing in a one-dimensional random-force field, a suitable model for the mechanical unzipping of the DNA double helix into single strands. Sinai's model is a special case ( $d = 0$ ) of the universal field theory of disordered elastic systems in  $d$  dimensions, where one can analytically calculate force correlations. The latter were measured in contact-line depinning ( $d = 1$ ) [7], Barkhausen noise ( $d = 2$ ) [8] and RNA-DNA peeling ( $d = 0$ ) [9]. While these experiments are for depinning, i.e. nonequilibrium, an experimental test of the equilibrium universality class is lacking. Here we test universality of equilibrium-force correlations as predicted by Sinai's model in DNA unzipping. The model parameters are naturally changed during the experiment allowing us to monitor the functional RG flow.

In the experiment, a DNA hairpin of 6.8k base pairs (BPs) is held between two beads. One is fixed at the tip of a micropipette, the other is optically trapped (Fig. 1(a) and Supp. Mat. Sec. A). By moving the optical trap at a speed  $v \approx 10$ nm/s, the double-stranded DNA (dsDNA) is mechanically pulled and converted into two single strands (ssDNA). The measured force-distance curve (FDC) shows a sawtooth pattern characteristic of stick-slip dynamics (Fig. 1(b), red curve). The hairpin unzips at a critical mean pinning force  $f_c \approx 15$ pN, fluctuating in the range 12-17pN. Once the hairpin is unzipped, the reverse process starts (Fig. 1(b), blue curve): the optical trap moves backward and the hairpin refolds into the dsDNA native conformation. The absence of hysteresis between reziping and unzipping FDCs and the fact that there is a single reaction coordinate, implies that the system is in equilibrium.

During unzipping, the base pair at the junction separating dsDNA from ssDNA is subject to random forces generated by the neighbouring monomers, and modeled by the motion of a

single particle ( $d = 0$ ) in a random potential that belongs to Sinai's universality class [6]. The number of unzipped BPs is a well-defined reaction coordinate. Opening (closing) one BP can be seen as a particle hopping to the right (left). We changed salt concentration from 10mM to 1000mM NaCl, Fig. 1(c), modulating the strength of BP interactions.

**The Model.** The motion of the base pair at the junction can be modeled by a Langevin equation (see Supp. Mat. Sec. B for the derivation)

$$\frac{\partial u}{\partial t} = m^2(w - u) + F(u) + \eta_u(t), \quad (1)$$

where  $u(t)$  is the extension of the molecular construct,  $w$  the relative trap-pipette position (Fig. 1(a)), and  $m^2$  the effective stiffness of the molecular construct. The random force is  $F(u) = -V'(u)$ , where  $V(u)$  is the free energy stored in the partially hybridized hairpin.  $F(u)$  acts at the hairpin junction and is determined by hydrogen bonding and stacking interactions between consecutive base pairs. Using the nearest-neighbour model one can show that these forces are random, and that their distribution is roughly a Gaussian (Supp. Mat. Sec. C). In equilibrium,  $\frac{\partial u}{\partial t} \approx 0$ , so the force  $F(u)$  applied to the hairpin in Eq. (1) is counteracted by the force  $F_w$  exerted on the bead by the optical trap. For a fixed trap position  $w$ ,  $F_w$  and  $u$  fluctuate due to the thermal noise and the BP breathing dynamics. The equilibrium force correlations are defined as,

$$\Delta_{m,T}(w - w') = \overline{F_w F_{w'}}^c = \overline{F_w F_{w'}} - \overline{F_w} \overline{F_{w'}}, \quad (2)$$

where  $\overline{(\dots)}$  stands for a double thermal and disorder average. Correlations depend on the value of  $m^2$ , through the  $m$ -dependence in Eq. (1). They also depend on temperature  $T$ , which leads to a rounding of  $\Delta_{m,T}(w)$  at small  $w$  (see below).

The FDCs in Figs. 1(b) and (c) show a sawtooth pattern characterized by segments of increasing force  $F_w$ , followed by abrupt drops caused by the cooperative unzipping of groups of base pairs in the range of 10-100 basepairs [11].

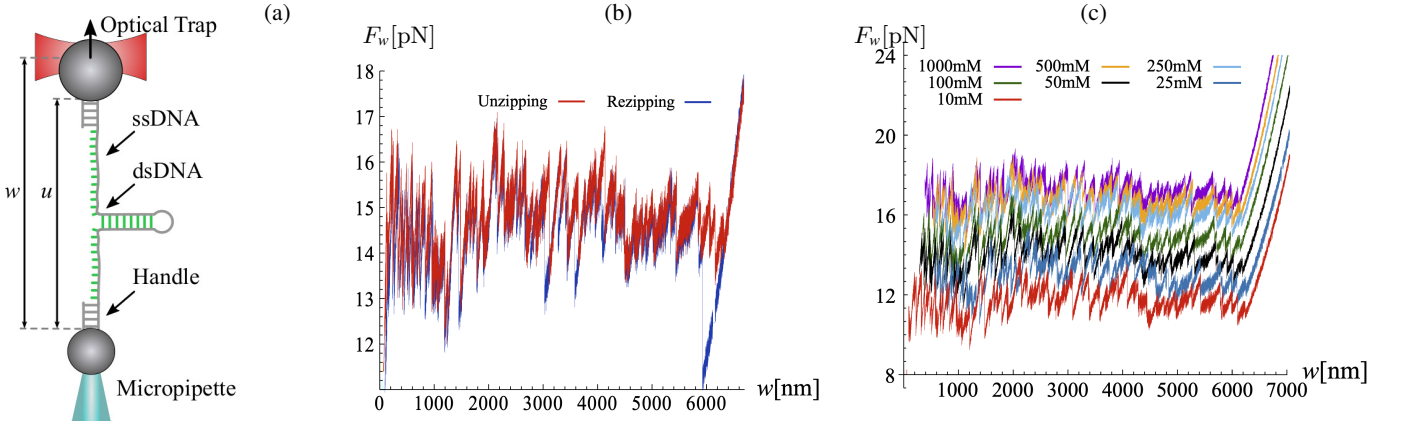


FIG. 1. (a) Experimental setup. (b) Unzipping (red) and rezipping (blue) FDC's demonstrating equilibrium behaviour. The residual hysteresis at the end of the FDC is due to the DNA end-loop that slows down the initiation of stem formation upon reconvolution. (c) Experimental FDC's,  $F_w$ , for various salt concentrations. The mean pinning force varies between 12-17pN, and is non-universal.

The slope of each segment, equivalent to the effective stiffness  $m^2$ , decreases with  $w$ , permitting us to measure the scaling of  $\Delta_{m,T}(w)$  with  $m^2$ . In fact,  $m^2$  depends on the combined effects of the optical trap, and the elastic response of the molecular construct (ssDNA and dsDNA handles). It can be written as (see Eq. (B27))

$$\frac{1}{m^2} = \frac{1}{k_b} + \frac{w}{\bar{z}_1 k_1}, \quad (3)$$

with  $k_b$  the trap stiffness, and  $\bar{z}_1, k_1$  the mean extension and stiffness of one nucleotide at the unzipping force. Modelling the elastic response of the hairpin [12] shows that  $k_1 \approx 130\text{pN/nm}$  and  $\bar{z}_1 \approx 0.45\text{nm}$  at the unzipping force  $f_c \approx 15\text{pN}$ , which gives a slope of about  $(\bar{z}_1 k_1)^{-1} \approx 0.02\text{pN}^{-1}$ . Eq. (3) implies that the larger the length of the unpaired DNA, the lower the effective stiffness  $m^2$ . To verify this, we split the FDCs into four regions (inset of Fig. 2). While smaller regions have smaller variations in  $m^2$ , regions must be taken sufficiently large for a reliable statistics. Eq. (3) agrees with the experimental data shown in Fig. 2.

Force correlations in Sinai's model can be framed in terms of the functional renormalisation group (FRG). The FRG arises as the field theory of disordered systems for interfaces [13–25], generalising the  $d = 0$  case described by the Sinai model. The FRG predicts two universality classes, critical depinning (non-equilibrium) and equilibrium (considered here). In equilibrium, the  $T \rightarrow 0$  limit of  $\Delta_{m,T}(w)$  in Eq. (2), can be written as

$$\Delta_m(w) = m^4 \rho_m^2 \tilde{\Delta}(w/\rho_m), \quad \rho_m \sim m^{-\zeta}, \quad (4)$$

with  $\tilde{\Delta}(w)$  the shape function,  $\zeta$  the roughness exponent, and  $w = w/\rho_m$  the rescaled dimensionless distance. The FRG allows for observables to be computed perturbatively in an expansion around the upper critical dimension, parameterised by  $\varepsilon = 4 - d$ . The shape function  $\tilde{\Delta}(w)$  is the fixed point of the FRG flow equation

$$0 = (\varepsilon - 2\zeta)\tilde{\Delta}(w) + \zeta w \tilde{\Delta}'(w) - \frac{1}{2} \partial_w^2 [\tilde{\Delta}(w) - \tilde{\Delta}(0)]^2 + \dots \quad (5)$$

The dots represent higher-loop corrections in  $\varepsilon$ , currently known up to 3-loop order [19–21, 23, 24, 26]. For the equilibrium random-field,  $\zeta = (4 - d)/3$ , which gives  $\zeta = 4/3$  for  $d = 0$ . This result is derived by integrating Eq. (5) from  $w = 0$  to  $w = \infty$ . It is exact to all orders in the loop expansion. Eq. (5) predicts that  $\tilde{\Delta}(w)$  has a cusp at  $w = 0$  which is rounded at finite  $T$ . Generalization of the FRG equation (5) to finite  $T$  allows us to estimate the size of the rounded region. An explicit relation between  $\Delta_m(w)$  and  $\Delta_{m,T}(w)$  was derived in [13–15],

$$\Delta_{m,T}(w) \approx \mathcal{N} \Delta_m(\sqrt{w^2 + t^2}), \quad t = \frac{6m^2 k_B T}{\varepsilon |\Delta'_m(0)|}. \quad (6)$$

It has been shown that the RG flow (5) preserves the area un-

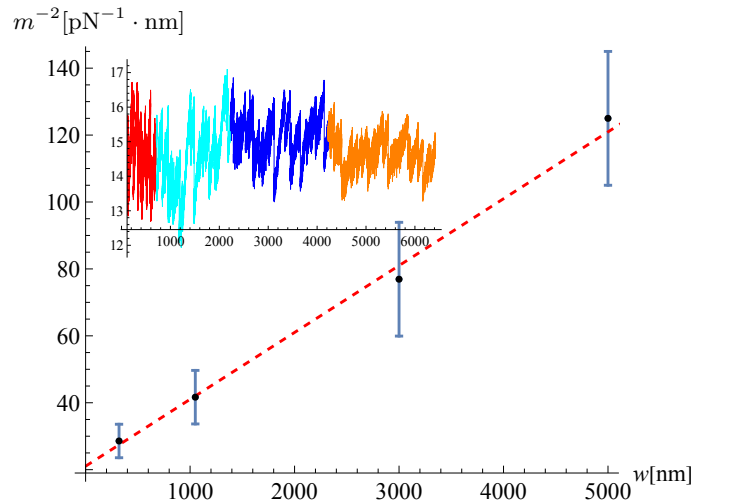


FIG. 2. Variation of the effective stiffness  $m^2$  versus  $w$  according to Eq. (3). The points correspond to the measured values of  $1/m^2$  for the four FDC regions (each one shown with a different colour in the inset). The fit to data (dashed line) and the extrapolation to  $w = 0$  gives the stiffness of the optical trap,  $k_b = 0.05 \pm 0.01\text{pN} \cdot \text{nm}^{-1}$ . The inset illustrates the four studied regions in a FDC at 1M NaCl.

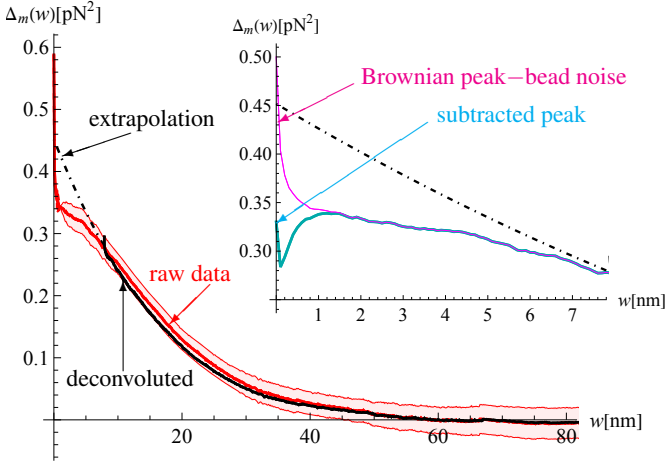


FIG. 3. Measured  $\Delta_{m,T}(w)$  for the first region (red).  $1\text{-}\sigma$  error is shown as a pink strip. Deconvolution (black solid) and extrapolation to  $w = 0$  (black dot-dashed). The inset shows  $\Delta_{m,T}(w)$  at short range with subtraction of the peak at  $w = 0$ , as explained in the main text.

der  $\Delta_{m,T}(w)$  for all  $T$  [26]. Therefore, we can use the measured  $\Delta_{m,T}(w)$  and Eq. (6) to determine the normalization factor  $\mathcal{N}$  and  $\Delta_m(w)$ . Details about the procedure are given in Supp. Mat. Sec. D.

For the Sinai model, the shape function  $\tilde{\Delta}$  in Eq. (5) is known analytically [13, 27],

$$\begin{aligned} \tilde{\Delta}(w) = & -\frac{e^{-\frac{w^3}{12}}}{4\pi^{\frac{3}{2}}\sqrt{w}} \int_{-\infty}^{\infty} d\lambda_1 \int_{-\infty}^{\infty} d\lambda_2 e^{-\frac{(\lambda_1-\lambda_2)^2}{4w}} \\ & \times e^{i\frac{w}{2}(\lambda_1+\lambda_2)} \frac{\text{Ai}'(i\lambda_1)}{\text{Ai}(i\lambda_1)^2} \frac{\text{Ai}'(i\lambda_2)}{\text{Ai}(i\lambda_2)^2} \\ & \times \left[ 1 + 2w \frac{\int_0^{\infty} dV e^{wV} \text{Ai}(i\lambda_1+V) \text{Ai}(i\lambda_2+V)}{\text{Ai}(i\lambda_1)\text{Ai}(i\lambda_2)} \right]. \end{aligned} \quad (7)$$

Here Ai is the Airy function, and  $\zeta = 4/3$  as in FRG.

**Data analysis.** We analysed 33 FDCs obtained by unzipping a 6.8kBP DNA hairpin in a broad range of salt conditions from 10mM to 1000mM NaCl at  $T = 298\text{K}$ . As illustrated in Fig. 2, we divided each FDC into four regions measuring the force correlations (2) for each region. Force correlations are equal within the experimental resolution for all salt conditions, as shown in Supplementary Fig. 7. Although the effective stiffness of the molecular construct  $m^2$  changes with salt, it changes much less than it does over the different unzipping regions for a fixed salt condition. To enlarge statistics we averaged  $\Delta_{m,T}(w)$  over all salts. Results for the first region are shown in Fig. 3 (red line with red strip for error bars).

To recover  $\Delta_{m,T}(w)$  in Eq. (6) we must subtract two sources of thermal noise, which are visible as a short-range correlated peak at  $w \approx 0$ : Brownian fluctuations of the bead; and the breathing dynamics (opening and closing) of the DNA base pairs at the junction. First, bead-noise subtraction reduces the peak's amplitude  $\Delta_{m,T}(w = 0)$  from  $\approx 0.6\text{pN}^2$  (red in main plot of Fig. 3) to  $\approx 0.5\text{pN}^2$  (magenta line in the inset). Second, we estimated the effect of the breathing

dynamics from numerical simulations of Sinai's model [26]. This reduces the peak from  $\approx 0.5\text{pN}^2$  to  $\approx 0.35\text{pN}^2$  with a dip of amplitude  $\approx 0.3\text{pN}^2$  for  $w < 1\text{nm}$  (cyan curve in the inset). This dip is also seen in simulations [26]. From  $\Delta_{m,T}(w)$  we derive the  $T = 0$  force correlations,  $\Delta_m(w)$ , by plotting the experimental data versus  $\sqrt{w^2 + t^2}$ , see Eq. (6), with  $t$  given there ( $T = 298\text{K}$ ,  $\varepsilon = 4$ ,  $m^2$  from Fig. 2). We initially estimate  $\Delta'_m(0)$  by extrapolation of the raw data. This gives  $\Delta_m(w)$  for  $w > t \approx 7\text{nm}$  (black continuous line in Fig. 3). The extrapolated  $\Delta_m(w)$  for  $w < t$  (dot-dashed region) is obtained by fitting a second-order polynomial (black dot-dashed line in Fig. 3). The whole procedure is iterated until convergence of  $\Delta_m(w)$  is reached. As a consistency check we used the  $T = 0$  theory prediction  $\Delta_m(w)$  together with Eq. (6) to calculate  $\Delta_{m,T}(w)$  for all regions, see Supp. Fig. 8.

Force correlations in Eq. (6) are described by three parameters: the correlation length  $\rho_m$  in the  $w$  direction, the stiffness  $m^2$  of the molecular construct, and the temperature  $T$ . With the measured value of  $m^2$  (Fig. 2) and  $k_B T = 4.11\text{pN} \cdot \text{nm}$  we use Eq. (6) to predict  $t$  ( $\varepsilon = 4$  and  $\Delta'_m(0)$  obtained from the small- $w$  extrapolation in Fig. 3). According to Eqs. (4) and (6), the scale  $\rho_m$  is the only fitting parameter, which we report on the table in Fig. 5 for all four regions. Its value increases with  $w$  indicating that FDCs become progressively less rough as unzipping progresses: For the first region,  $\rho_m = 26.8\text{nm}$ , which corresponds to 33 basepairs [12], the typical size of avalanches that can be resolved in the FDC at the beginning of the unzipping process.

We now check two predictions of the theory: the result (7) and the FRG scaling relation (4). In particular, the scaling function  $\tilde{\Delta}$  only depends on the dimensionless combination  $w/\rho_m \sim wm^\zeta$ , and its amplitude is universal. The inset of Fig. 4 shows  $\Delta_m(w)$  for the four regions where  $\rho_m$  increases while the molecule is unzipped and  $m^2$  decreases. In Fig. 4 we test the scaling law (4) with  $\zeta = 4/3$ , as predicted for Sinai's model. We can also determine the value of  $\zeta$  independently of the collapse in Fig. 4. In Fig. 5 we show results for the scaling of the correlation length  $\rho_m$  and amplitude  $\Delta_m(0)$  with  $m$ . We get  $\zeta = 1.41 \pm 0.10$  and  $\zeta = 1.29 \pm 0.08$  from the scaling of  $\rho_m$  and  $\Delta_m(0)$ , respectively, giving an average of  $\zeta = 1.34 \pm 0.06$  in agreement with the expected value  $\zeta = 4/3$ . Details are given in Supp. Fig. 8.

We can go one step further: In random-field systems, the correlations of the potential  $V(u)$  grow linearly at large  $u$ -distances,  $\frac{1}{2}[V(u) - V(u')]^2 \simeq \sigma|u - u'|$ . The constant  $\sigma$  is related to the force correlator  $\Delta_m$  by

$$\sigma = \int_0^{\infty} \Delta_{\infty}(u) du \equiv \int_0^{\infty} \Delta_m(w) dw. \quad (8)$$

This relation holds for the microscopic  $\Delta_{\infty}(u)$  and the measured  $\Delta_m(w)$ , as the area under  $\Delta_m(w)$  is preserved by the RG flow, as previously discussed. A constant  $\sigma$  in Eq. (8) implies  $\zeta = 4/3$  for all  $m$  in Eq. (4). Eq. (8) then yields the analytic prediction

$$\rho_m = \left[ \frac{\int_{w>0} \Delta_{\infty}(w)}{m^4 \int_{w>0} \tilde{\Delta}(w)} \right]^{1/3}. \quad (9)$$

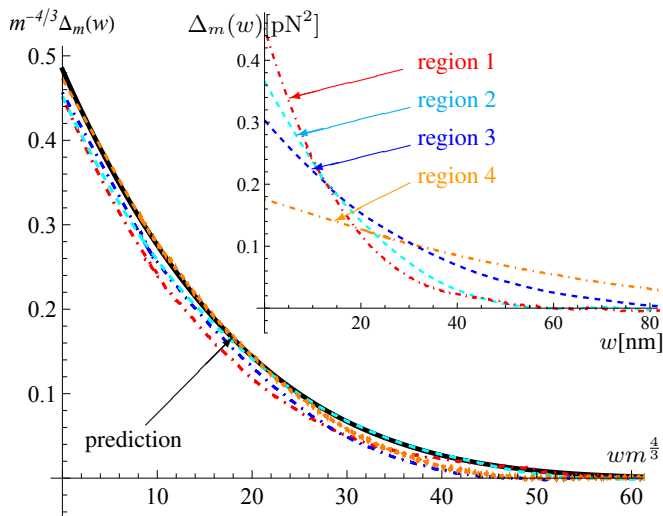


FIG. 4. Inset: The function  $\Delta_m(w)$  for the four regions changes with the measured  $m$  (see Fig 5). Main: Collapse of  $\Delta_m(w)$  according to Eq. (4) with  $\zeta = 4/3$ . In black we show the theoretical  $\Delta_m(w)$ , with  $\rho_m = 29(3)\text{nm}$  as predicted by the microscopic disorder.

| Observable                            | region 1 | region 2   | region 3     | region 4    |
|---------------------------------------|----------|------------|--------------|-------------|
| $w[\text{nm}]$                        | [0, 800] | [800,2200] | [2200, 4200] | [4200,6200] |
| $m^2[\text{pN/nm}]$                   | 0.036(3) | 0.027(3)   | 0.016(4)     | 0.007(4)    |
| $\rho_m [\text{nm}]$                  | 27(3)    | 29(3)      | 42(4)        | 76(5)       |
| $\Delta_m(0)[\text{pN}^2]$            | 0.44     | 0.38       | 0.31         | 0.18        |
| $\Delta'_m(0)[\text{pN}^2/\text{nm}]$ | 0.032    | 0.018      | 0.0099       | 0.0032      |

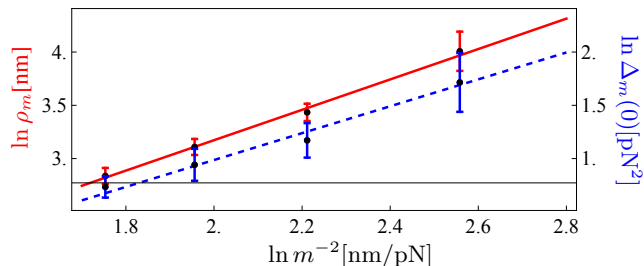


FIG. 5. Top: Properties of the force correlator for the four regions in Fig. 2. The correlation length  $\rho_m = C\Delta_m(0)/\Delta'_m(0)$ , with  $C = \tilde{\Delta}_m(0)/\tilde{\Delta}'_m(0) = 1.36$ , see Eq. (7). Bottom: The scaling with  $m$  of  $\rho_m$  (red, solid),  $\zeta = 1.41 \pm 0.10$ , and  $\Delta_m(0)$  (blue dashed),  $\zeta = 1.29 \pm 0.08$ . Their mean  $\zeta = 1.34 \pm 0.06$  agrees with the expected value,  $\zeta = 4/3$ .

In Supp. Mat. Sec. C, we discuss how the microscopic correlator  $\Delta_\infty(w)$  can be obtained from the binding energies, using our estimate of  $\Delta_\infty(0) \approx 10(2)\text{pN}^2$ , which decays to half this value for BP distance 1, and to 0 for BP distance 2, corresponding to 1.6nm. A linear interpolation of  $\Delta_\infty(u)$  between these values gives  $\sigma = 8(2)\text{pN}^2 \cdot \text{nm}$  in Eq. (8). Using

$\int_{w>0} \tilde{\Delta}(w) = 0.252$  from Eq. (7), and substituting in Eq. (9) gives  $\rho_m = 29(3)\text{nm}$  for region 1 in agreement with the value previously obtained ( $\rho_m \approx 27\text{nm}$  for  $m^2 = 0.036 \text{ pN/nm}$  in Fig. 5). In Fig. 4 (main) we show the predicted force correlator (black curve) with the predicted  $\rho_m = 29(3)\text{nm}$ .

**Conclusions.** We tested Sinai's model of equilibrium force correlations and their universality in DNA unzipping experiments. In DNA the binding energies between base pairs are correlated up to two base pairs, making it a suitable realization of Sinai's model. We experimentally measured the roughness exponent  $\zeta$  finding agreement with Sinai's prediction,  $\zeta = 4/3$ . While predictions for critical exponents are commonplace, far more difficult is to predict the amplitude and the correlation length of correlation functions in critical phenomena. Here we show that the amplitude of force correlations and its correlation length can be predicted from the effective stiffness of the molecular construct  $m^2$  and the energy parameters of the nearest-neighbour model in DNA thermodynamics [28, 29]. We get experimental values for  $\rho_m$  that are within 10% of the predicted ones: e.g. for region 1,  $\rho_m \approx 27\text{nm}$  (measured) versus  $\rho_m \approx 29\text{nm}$  (predicted).

It is interesting to compare our unzipping experiment to the peeling of complementary RNA-DNA strands [9]. Peeling is a highly irreversible process belonging to the depinning universality class. It is characterized by a significantly larger effective stiffness  $m^2$ , and a larger correlation length of about 186 BP as compared to the 26 to 77 BP of DNA unzipping. The high energies required for DNA peeling make the  $T = 0$  nonequilibrium depinning transition relevant there, whereas for DNA unzipping thermal fluctuations occur in equilibrium.

Our study can be extended to DNA with chemically modified bases and RNA [30]. It would also be interesting to study DNA sequences with long-range correlations [31] and with periodically repeated motifs, a physical realization of periodic disorder relevant for charge-density waves. Finally, one could consider dynamical effects, e.g. upon temperature changes [32] using a temperature-jump optical trap [33]. Overall, single-molecule unzipping offers exciting possibilities to experimentally investigate critical phenomena in random polymers.

**Acknowledgements.** C. ter Burg and K. Wiese were supported by LabEx ENS-ICFP. P.R. was supported by the Angelo della Riccia foundation. M.R.-P. and F. R. were supported by Spanish Research Council Grant PID2019-111148GB-I00 and F. R. by the Institució Catalana de Recerca i Estudis Avançats, Academia Prize 2018.

**Author contributions.** C.T.B and K.J.W developed the field theory. F.R. derived the equation of motion from the experimental model. C.T.B analysed the data. P.R. obtained the experimental data and M.R. set the optical tweezer instrument. All authors contributed to the writing of the paper.

[1] J.-P. Bouchaud and A. Georges, *Anomalous diffusion in disordered media: statistical mechanisms, models and physical ap-*

*plications*, *Phys. Rep.* **195** (1990) 127-293.



- [2] M. Kardar, *Nonequilibrium dynamics of interfaces and lines*, *Phys. Rep.* **301** (1998) 85–112.
- [3] T. R. Kirkpatrick and D. Thirumalai, *Colloquium: Random first order transition theory concepts in biology and physics*, *Rev. Mod. Phys.* **87** (2015) 183.
- [4] E. Schrödinger, *What is life?*, Cambridge University Press (1944).
- [5] D.P. Varn and J.P. Crutchfield, *What did Erwin mean? The physics of information from the materials genomics of aperiodic crystals and water to molecular information catalysts and life*, *Philos. Trans. Royal Soc. A* **374-2063** (2016) 20150067.
- [6] Y.G. Sinai, *The limiting behaviour of a one-dimensional random walk in a random environments*, *Theory Probab. Appl.* **27** (1983) 256–268.
- [7] P. Le Doussal, K.J. Wiese, S. Moulinet and E. Rolley, *Height fluctuations of a contact line: A direct measurement of the renormalized disorder correlator*, *EPL* **87** (2009) 56001, arXiv:0904.4156.
- [8] C. ter Burg, F. Bohn, F. Durin, R.L. Sommer and K.J. Wiese, *Force correlations in disordered magnets*, *Phys. Rev. Lett.* **129** (2022) 107205, arXiv:2109.01197.
- [9] K.J. Wiese, M. Bercy, L. Melkonyan and T. Bizebard, *Universal force correlations in an RNA-DNA unzipping experiment*, *Phys. Rev. Research* **2** (2020) 043385, arXiv:1909.01319.
- [10] Supplemental Material for this letter, see page 6.
- [11] J. M. Huguët, N. Forns and F. Ritort, *Statistical properties of metastable intermediates in DNA unzipping*, *Phys. Rev. Lett.* **103** (2009) 248106.
- [12] A. Alemany and F. Ritort, *Determination of the elastic properties of short ssDNA molecules by mechanically folding and unfolding DNA hairpins*, *Biopolymers* **101** (2014) 1193–1199.
- [13] K.J. Wiese, *Theory and experiments for disordered elastic manifolds, depinning, avalanches, and sandpiles*, *Rep. Prog. Phys.* **85** (2022) 086502 (133pp), arXiv:2102.01215.
- [14] L. Balents and P. Le Doussal, *Thermal fluctuations in pinned elastic systems: field theory of rare events and droplets*, *Ann. Phys. (NY)* **315** (2005) 213–303, cond-mat/0408048.
- [15] P. Chauve, T. Giamarchi and P. Le Doussal, *Creep and depinning in disordered media*, *Phys. Rev. B* **62** (2000) 6241–67, cond-mat/0002299.
- [16] D.S. Fisher, *Interface fluctuations in disordered systems:  $5 - \varepsilon$  expansion*, *Phys. Rev. Lett.* **56** (1986) 1964–97.
- [17] T. Nattermann, S. Stepanow, L.-H. Tang and H. Leschhorn, *Dynamics of interface depinning in a disordered medium*, *J. Phys. II (France)* **2** (1992) 1483–8.
- [18] O. Narayan and D.S. Fisher, *Threshold critical dynamics of driven interfaces in random media*, *Phys. Rev. B* **48** (1993) 7030–42.
- [19] P. Chauve, P. Le Doussal and K.J. Wiese, *Renormalization of pinned elastic systems: How does it work beyond one loop?*, *Phys. Rev. Lett.* **86** (2001) 1785–1788, cond-mat/0006056.
- [20] P. Le Doussal, K.J. Wiese and P. Chauve, *2-loop functional renormalization group analysis of the depinning transition*, *Phys. Rev. B* **66** (2002) 174201, cond-mat/0205108.
- [21] P. Le Doussal, K.J. Wiese and P. Chauve, *Functional renormalization group and the field theory of disordered elastic systems*, *Phys. Rev. E* **69** (2004) 026112, cond-mat/0304614.
- [22] P. Le Doussal, K.J. Wiese, E. Raphael and R. Golestanian, *Can nonlinear elasticity explain contact-line roughness at depinning?*, *Phys. Rev. Lett.* **96** (2006) 015702,
- [23] K.J. Wiese, C. Husemann and P. Le Doussal, *Field theory of disordered elastic interfaces at 3-loop order: The  $\beta$ -function*, *Nucl. Phys. B* **932** (2018) 540–588, arXiv:1801.08483.
- [24] C. Husemann and K.J. Wiese, *Field theory of disordered elastic interfaces to 3-loop order: Results*, *Nucl. Phys. B* **932** (2018) 589–618, arXiv:1707.09802.
- [25] R.B.A. Zinati, C. Duclut, S. Mahdisoltani, A. Gambassi and R. Golestanian, *Stochastic dynamics of chemotactic colonies with logistic growth*, *EPL* **136** (2022) 50003,
- [26] C. ter Burg and K.J. Wiese, *Force-force correlator for driven disordered systems at finite temperature*, (2022), arXiv:2201.12652v1.
- [27] P. Le Doussal, *The Sinai model in presence of dilute absorbers*, *J. Stat. Mech.* (2009) P07032, arXiv:0906.0267.
- [28] M. Zuker, *Mfold web server for nucleic acid folding and hybridization prediction*, *Nucleic Acids Res.* **31** (2003) 3406–15.
- [29] R. Lorenz, S.H. Bernhart, C. Höner zu Siederdisen, H. Tafer, C. Flamm, P.F. Stadler and I.L. Hofacker, *ViennaRNA package 2.0*, *Algorithms for Molecular Biology* **6** (2011).
- [30] P. Rissone, C.V. Bizarro, and F. Ritort, *Stem-loop formation drives RNA folding in mechanical unzipping experiments*, *Proc. Natl. Acad. Sci. U.S.A.* **119**, e2025575119 (2022).
- [31] M. Slutsky, M. Kardar and L. A. Mirny, *Diffusion in correlated random potentials, with applications to DNA*, *Phys. Rev. E* **69** (2004) 061903.
- [32] M. Sales, J. P. Bouchaud and F. Ritort, *Temperature shifts in the Sinai model: static and dynamical effects*, *J. Phys. A* **t 36** (2003) 665–684.
- [33] S. De Lorenzo, M. Ribezzi-Crivellari, J. Arias-Gonzalez, S. B. Smith and F. Ritort, *A temperature-jump optical trap for single-molecule manipulation*, *Biophys. J.* **108** (2015) 2854–2864.
- [34] J.M. Huguët, M. Ribezzi-Crivellari, C.V. Bizarro and F. Ritort, *Derivation of nearest-neighbor DNA parameters in magnesium from single molecule experiments*, *Nucleic Acids Res.* **45** (2017) 12921–12931,
- [35] J.M. Huguët, C.V. Bizarro, N. Forns, S.B. Smith, C. Bustamante, and F. Ritort, *Single-molecule derivation of salt dependent base-pair free energies in DNA*, *Proc. Natl. Acad. Sci* **107** (2010) 15431–15436, arXiv:1010.1188.

## Experimental test of Sinai's model in DNA unzipping

### Supplementary Material

Cathelijne ter Burg<sup>1</sup>, Paolo Rissone<sup>2</sup>, Marc Rico-Pasto<sup>2</sup>, Felix Ritort<sup>2,3</sup> and Kay Jörg Wiese<sup>1</sup>

<sup>1</sup>*Laboratoire de Physique de l'École Normale Supérieure, ENS, Université PSL, CNRS, Sorbonne Université, Université Paris-Diderot, Sorbonne Paris Cité, 24 rue Lhomond, 75005 Paris, France.*

<sup>2</sup>*Small Biosystems Lab, Condensed Matter Physics Department, Universitat de Barcelona, Carrer de Martí i Franquès 1, 08028 Barcelona, Spain.*

<sup>3</sup>*Institut de Nanociència i Nanotecnologia (IN2UB), Universitat de Barcelona, 08028 Barcelona, Spain*

#### Section A: Experimental details

We use laser optical-tweezers (LOT) to unzip a 6.8k base-pair (BPs) DNA hairpin consisting of a stem of fully complementary Watson-Crick base-pairs ending with a tetra-loop ACTA. The hairpin strands are terminated with short (29 BP) double-stranded DNA (dsDNA) handles, one labeled with a digoxigenin tail (DIG) and one with a biotin tail (BIO). In our setup the DIG-labeled and BIO-labeled handles are tethered to anti-DIG (AD) and streptavidin-coated (SA) beads, respectively. The AD bead is optically trapped while the SA one is held by air suction at the tip of a glass micro-pipette. In a typical unzipping experiment, the optical trap is repeatedly moved back and forth relative the fixed micro-pipette at a constant loading rate. At the initial trap position, the molecule starts in its folded dsDNA configuration (Fig. 6(a)). As the optical trap is moved away from the pipette the unzipping reaction proceeds and the molecule gradually unzips (Fig. 6(a)) until it is completely unfolded and the two single-strands (ssDNA) are fully stretched (Fig. 6(c)). At this point the reverse reaction starts (re-zipping) and the molecule steadily refolds into its dsDNA form (dashed arrows). The force versus trap position  $F(w)$  sampled during this process shows a saw-tooth pattern which depends on the DNA hairpin sequence. The fact that the unzipping and re-zipping saw-tooth force-distance curves coincide (Fig. 6 (b)) means that the processes are in equilibrium. Here, we unzipped/rezipped the 6.8kpbs DNA hairpin at room temperature (298K) in a wide range of monovalent salt conditions (10mM, 25mM, 50mM, 100mM, 250mM, 500mM and 1000mM NaCl). Fig. 6 (c) shows unzipping curves for a range of different salt concentrations.

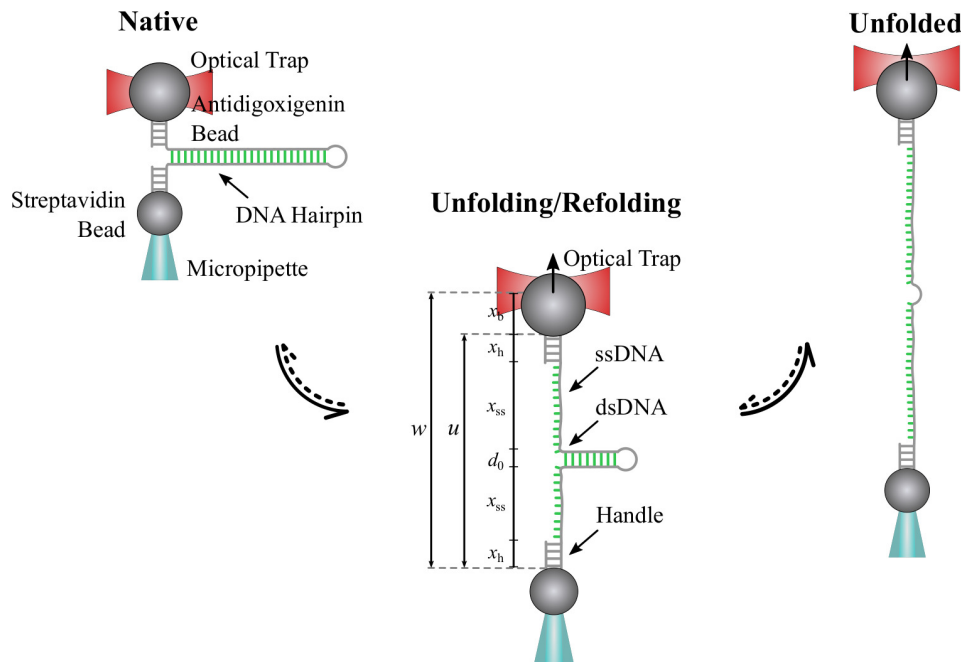


FIG. 6. Schematic description of the unzipping experiment as reported Supp. Mat. Sec. A and representation of the parameters introduced in the computation in Supp. Mat. Sec. B. As reported in the text,  $x_h$  is the extension of the handles,  $x_b$  is the displacement of the bead from the center of the optical trap,  $d_0$  is the diameter of the folded double-helix ( $\sim 2$ nm) and  $x_{ss}$  is the extension of the ssDNA.

## Section B: Model for the unzipping experiment

Given the setup in Fig. 6 (middle panel), at a fixed trap-pipette distance  $w$  one can write

$$w = x_b + u, \quad (\text{B1})$$

where  $x_b$  is the distance of the bead from the center of the optical trap and  $u$  is the total length of the molecular construct. The latter can be written as

$$u = 2x_h + d_0 + 2x_{ss}(n), \quad (\text{B2})$$

where  $x_h$  is the extension of the dsDNA handle,  $d_0$  is the diameter of the hybridized hairpin and  $x_{ss}(n)$  is the extension of the ssDNA. The molecular construct has two short handles, each of  $29\text{BP} \equiv 10\text{nm}$  in length, much shorter than the persistence length of dsDNA (50 nm) and are very rigid at the unzipping force ( $\approx 15\text{pN}$ ). Moreover, their overall extension is negligible compared to  $x_{ss}(n)$ . Also we can neglect  $d_0 \approx 2\text{nm}$ . The total length of the molecular construct can be approximated as

$$u \simeq 2x_{ss}(n) \equiv 2nz, \quad (\text{B3})$$

with  $2n$  the total number of unzipped bases and

$$z = z(u, n) = \frac{u}{2n}, \quad (\text{B4})$$

the monomer extension. The total energy is given by

$$\mathcal{H}_w(u, n) = \frac{1}{2}k_b(w - u)^2 + 2n\hat{U}\left(\frac{u}{2n}\right) + G_{N-n}. \quad (\text{B5})$$

The first term is the harmonic potential of the optical trap with stiffness  $k_b$ . The second term,  $U_{ss}(u, 2n) = 2n\hat{U}(z)$  is the elastic energy of the ssDNA that behaves as an ideal elastic model.  $G_{N-n}$  is the binding energy of the  $N - n$  base pairs in the stem.

Given (B5) and  $w$  fixed,  $u$  and  $n$  are the only two degrees of freedom of the system. Their respective equations of motion are

$$\gamma_u \frac{\partial u}{\partial t} = -\frac{\partial \mathcal{H}_w}{\partial u} + \eta_u, \quad (\text{B6a})$$

$$\gamma_n \frac{\partial n}{\partial t} = -\frac{\partial \mathcal{H}_w}{\partial n} + \eta_n, \quad (\text{B6b})$$

where  $\gamma_u$  and  $\gamma_n$  are constants (viscosities), and  $\eta_u$  and  $\eta_n$  are  $\delta$ -correlated Brownian noises with correlations  $\langle \eta_u(t)\eta_u(t') \rangle = \langle \eta_n(t)\eta_n(t') \rangle = 2k_B T \delta(t - t')$ . Mechanical equilibrium for the bead implies

$$-\frac{\partial \mathcal{H}_w}{\partial u} = 0 \Rightarrow k_b(w - u) = f_1\left(\frac{u}{2n}\right), \quad (\text{B7})$$

where  $f_1(z) = -\hat{U}'(z)$  is the force acting on the ssDNA. Note that the timescale for  $u$  is much faster than the time scale for  $n$ , so we can take  $u$  in equilibrium and Eq. (B7) holds. This allows us to set  $\eta_n \rightarrow 0$ .

For a given  $w$  and  $n$ , there is an equilibrium position  $u^*(w, n)$  for which the force exerted by the optical trap on the bead equals the force exerted by the molecular construct on the bead. For the basepair dynamics we find

$$\begin{aligned} -\frac{\partial \mathcal{H}_w}{\partial n} &= -2\hat{U}\left(\frac{u}{2n}\right) + \frac{u}{n}\hat{U}'\left(\frac{u}{2n}\right) + G'_{N-n} \\ &= -2\hat{U}(z) + 2z\hat{U}'(z) + G'_{N-n} \\ &= 2 \int_0^z f_1(z')dz' - 2zf_1(z) + G'_{N-n} \\ &= -2 \int_0^{f_1(z)} z(f')df' + G'_{N-n} \\ &= I_w(f(n)) + G'_{N-n}, \end{aligned} \quad (\text{B8})$$

where

$$I_w(f) := -2 \int_0^f z(f')df'. \quad (\text{B9})$$

For a given  $w$  and  $u^*(w, n)$ , there is an equilibrium  $n^*$ , so that Eq. (B8) gives

$$-\left. \frac{\partial \mathcal{H}_w(n)}{\partial n} \right|_{n^*} = I_w(n^*) + G'(N - n^*) = 0 \Rightarrow I_w(n^*) = -G'(N - n^*), \quad (\text{B10})$$

where  $n^*$  is the value at which the absolute minimum is attained. Expanding  $I_w(n)$  around  $n^*$  and substituting the previous result one gets

$$I_w(n) = I_w(n^*) + \left. \frac{\partial I_w}{\partial n} \right|_{n^*} (n - n^*) + \mathcal{O}(n - n^*)^2 \quad (\text{B11})$$

$$= -G'(N - n^*) + \left. \frac{\partial I_w}{\partial n} \right|_{n^*} (n - n^*) + \mathcal{O}(n - n^*)^2. \quad (\text{B12})$$

Let us focus on the first-order term. Using Eq. (B9), it can be rewritten as

$$\frac{\partial I_w}{\partial n} = \frac{\partial I_w(n)}{\partial f_1} \frac{\partial f_1}{\partial n} = -2z_1 \frac{\partial f_1}{\partial n}, \quad (\text{B13})$$

where  $z_1 := z(f_1)$ . Taking a derivative w.r.t.  $n$  of Eq. (B7) we obtain

$$-k_b \frac{\partial u}{\partial n} = \frac{\partial f_1\left(\frac{u}{2n}\right)}{\partial n} = k_1 \left(\frac{u}{2n}\right) \left[ \frac{1}{2n} \frac{\partial u}{\partial n} - \frac{u}{2n^2} \right], \quad (\text{B14})$$

where

$$k_1 \equiv k_1(z) := f_1'(z). \quad (\text{B15})$$

Solving for  $\frac{\partial u}{\partial n}$  yields

$$\frac{\partial u}{\partial n} = \frac{k_1 u}{n(2nk_b + k_1)}. \quad (\text{B16})$$

Using Eq. (B13), and the first equality of Eq. (B14) gives

$$\frac{\partial I_w}{\partial n} = -2z_1 \frac{\partial f_1}{\partial n} = -2z_1 k_b \frac{\partial u}{\partial n} = -\frac{2z_1 k_b k_1 u}{n(2nk_b + k_1)} = -\frac{4z_1^2 k_b k_1}{k_1 + 2nk_b}. \quad (\text{B17})$$

The equation of motion for the basepairs dynamics in Eq. (B6b) can therefore be written as

$$\begin{aligned} \gamma_n \frac{\partial n}{\partial t} &= I_w(n) + G'(N - n) + \eta_n \simeq I_w(n^*) + \left. \frac{\partial I_w(n)}{\partial n} \right|_{n=n^*} (n - n^*) + G'(N - n) + \eta_n \\ &= \left. \frac{\partial I_w}{\partial n} \right|_{n=n^*} (n - n^*) - G'(N - n^*) + G'(N - n) + \eta_n \\ &= -\frac{4z_1^2 k_b k_1}{k_1 + 2nk_b} (n - n^*) - G'(N - n^*) + G'(N - n) + \eta_n. \end{aligned} \quad (\text{B18})$$

Define

$$G(N - n) = \sum_{i=N-n}^N g_i. \quad (\text{B19})$$

The random forces are

$$f_n = -G'(N - n) = -g_{N-n} \equiv -g(N - n). \quad (\text{B20})$$

We observe that

$$u = 2\langle z_1 \rangle n, \quad u^* = 2\langle z_1 \rangle n^*, \quad \frac{\partial n}{\partial t} = \frac{1}{2\langle z_1 \rangle} \frac{\partial u}{\partial t}, \quad (\text{B21})$$

where  $\langle z_1 \rangle$  denotes a statistical average over  $z_1$ .



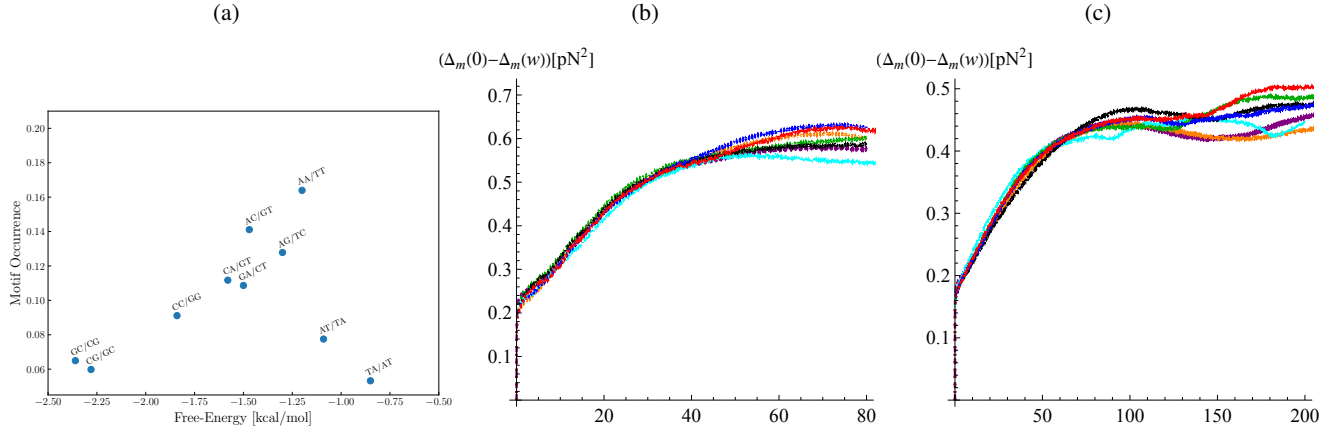


FIG. 7. (a) Distribution of the nearest-neighbour binding energies at 1M NaCl salt concentration for the 6 kBP sequence studied here. For the first (b) and third (c) region, the averaged  $\Delta_m$  for each salt concentration. Despite the dependence of the pinning force on the salt concentration, the correlation length is not visibly affected by the salt concentration. Color code as in Fig. 1 (c).

The final equation of motion for  $u$  can be rewritten as

$$\tilde{\gamma}_n \frac{\partial u}{\partial t} = m^2(u^* - u) + F(u) - F(u^*) \quad (\text{B22})$$

$$\equiv m^2(w - u) + F(u), \quad (\text{B23})$$

where

$$w = u^* - \frac{1}{m^2} F(u^*), \quad (\text{B24})$$

$$\tilde{\gamma}_n = \frac{\gamma_n}{4\langle z_1 \rangle^2}, \quad (\text{B25})$$

$$F(u) = -2\langle z_1 \rangle g\left(N - \frac{u}{2\langle z_1 \rangle}\right), \quad (\text{B26})$$

$$\frac{1}{m^2} = \frac{1}{k_b} + \frac{2n}{k_1} \approx \frac{1}{k_b} + \frac{u}{\langle z_1 \rangle k_1} \approx \frac{1}{k_b} + \frac{w}{\langle z_1 \rangle k_1}. \quad (\text{B27})$$

Note that  $u^*$  in this equation is simply a *minimum*, not necessarily the previously assumed global minimum. Rescaling  $t$ , we set  $\tilde{\gamma}_n \rightarrow 1$ . Noticing that  $u$  and  $w$  in the experiment are defined up to an overall shift gives equation (1) in the main text.

### Section C: Distribution of binding energies

In Ref. [34, 35] the base-pair free energies in DNA were experimentally determined for the 6kBP sequence studied in this paper. Fig. 7(a) shows that the distribution of basepair energies is roughly Gaussian, here given for the 1M salt concentration. Using these binding energies one can evaluate the microscopic disorder  $\Delta_\infty(w)$ . One uses that 1kcal/mol = 6.944pN · nm and converts to forces by dividing by the base-pair length of  $\approx 0.8\text{nm}$  [12]. The resulting  $\Delta_\infty(w)$  decays to zero on a scale of 2BP  $\approx 1.6\text{ nm}$ .

The FRG implies that  $\int_{w>0} \Delta(w)$  is independent of  $m^2$ . As a consequence

$$\begin{aligned} \int_0^\infty dw \Delta_\infty(w) &\equiv \int_0^\infty dw \Delta_m(w) \\ &= \int_0^\infty dw m^4 \rho_m^2 \tilde{\Delta}_m(w/\rho_m) = m^4 \rho_m^3 \int_0^\infty dw \tilde{\Delta}_m(w) = 0.252 m^4 \rho_m^3. \end{aligned} \quad (\text{C1})$$

Solving for  $\rho_m$  yields Eq. (9) presented in the main text,

$$\rho_m = \left[ \frac{\int_{w>0} \Delta_\infty(w)}{m^4 \int_{w>0} \tilde{\Delta}(w)} \right]^{1/3} \simeq \left[ \frac{3.97}{m^4} \int_{w>0} \Delta_\infty(w) \right]^{1/3}. \quad (\text{C2})$$

The equality (C1) is satisfied in our experiment, a strong test of universality. We find  $\int_{w>0} \Delta_m(w) \approx 7.2(4)\text{pN}^2 \cdot \text{nm}$ , for the first region,  $\int_{w>0} \Delta_m(w) \approx 7.0(4)\text{pN}^2 \cdot \text{nm}$  for the second,  $\int_{w>0} \Delta_m(w) \approx 7.0(5)\text{pN}^2 \cdot \text{nm}$  for the third and  $\int_{w>0} \Delta_m(w) \approx 7.2(7)\text{pN}^2 \cdot \text{nm}$  for the last region. Our estimate of the microscopic  $\int_{w>0} \Delta_\infty(w)$  comes close to this. If we use the binding energies of [34] for the 1M salt concentration, we find  $\int_{w>0} \Delta_\infty(w) \approx 8(2)\text{pN}^2 \cdot \text{nm}$  [34, 35]. For the first region this corresponds to  $\rho_m = 29(3)\text{nm}$  close to the experimentally measured value of  $27(3)\text{nm}$ .

### Salt dependence

The base-pair energies change with the salt concentration according to

$$dG([\text{salt}]) = dG_0([1\text{M}]) - m_i \ln([\text{salt}]), \quad (\text{C3})$$

where  $dG_0$  is the binding energy at a 1M salt concentration. The values for  $m_i$  are given in Table 1 of Ref. [35]. Values for  $\int_{w>0} \Delta_\infty(w)$  for different salt concentrations are given in Table I. One can do a similar analysis, taking into account the proportion of samples per salt concentration. One finds a somewhat larger value  $\int_{w>0} \Delta_\infty(w) \approx 9(2)\text{pN}^2 \cdot \text{nm}$  and  $\rho_m = 30(3)\text{nm}$ , still in agreement within error bars.

| salt concentration [mM] | $\int_{w>0} \Delta_\infty(w)$ | # samples |
|-------------------------|-------------------------------|-----------|
| 1000                    | 8(2)                          | 6         |
| 500                     | 8(2)                          | 7         |
| 250                     | 8(2)                          | 5         |
| 100                     | 9(2)                          | 5         |
| 50                      | 9(2)                          | 4         |
| 25                      | 10(3)                         | 3         |
| 10                      | 10(3)                         | 3         |

TABLE I. Properties of the microscopic disorder using the binding energies of [35]. In our analysis, we averaged over the different salt concentrations (see main text). The resulting error is small, of the order of 2BP on the total correlation length.

### Section D: RG at finite temperature, rounding and deconvolution

At finite temperature, the 1-loop FRG equation without rescaling acquires an additional term

$$-m\partial_m \Delta_m(w) = -\frac{1}{2}\partial_w^2 [\Delta_m(w) - \Delta_m(0)]^2 + \tilde{T}_m \Delta_m''(w) \dots \quad (\text{D1})$$

In Eq. (5) we have written the fixed-point equation for the rescaled version  $\tilde{\Delta}(w) = m^{\varepsilon-2\zeta} \Delta(wm^\zeta)$ ,

$$-m\partial_m \tilde{\Delta}(w) = (\varepsilon-2\zeta)\tilde{\Delta}(w) + \zeta w \tilde{\Delta}'(w) - \frac{1}{2}\partial_w^2 [\tilde{\Delta}(w) - \tilde{\Delta}(0)]^2 + \tilde{T}_m \tilde{\Delta}''(w) \dots \quad (\text{D2})$$

What is remarkable about Eq. (D1) is that the RG flow conserves the integral  $\int_{w>0} \Delta(w)$ , both at vanishing temperature  $\tilde{T}_m = 0$  and at  $\tilde{T}_m > 0$ . The reason is that the r.h.s. of Eq. (D1) is a total derivative. For the random field solution  $\zeta = \varepsilon/3$  relevant for us, this also holds for the rescaled Eq. (D2).

In Eq. (6) we wrote the finite-temperature solution in the standard form

$$\Delta_{m,T}(w) \approx \mathcal{N} \Delta_m(\sqrt{w^2 + t^2}), \quad t = \frac{6m^2 k_B T}{\varepsilon |\Delta_m'(0)|}. \quad (\text{D3})$$

As the flow preserves the area, it is important to fix  $\mathcal{N}$ , s.t. the integrals on both sides coincide. This adds a non-trivial change in normalization, which cannot be given in closed form. Another problem with Eq. (D3) is that given  $\Delta_{m,T}(w)$ , one can reconstruct  $\Delta_m(w)$  only for  $w \geq t$ . Since this is a phenomenological approximation, we may propose a different approximation. Namely, to obtain the finite- $t$  solution by convoluting the zero-temperature solution with an appropriately chosen diffusion kernel,

$$\Delta_{m,T}(w) = \int_{-\infty}^{\infty} du \Delta_m(u) R(u-w, \tau), \quad R(u, \tau) = \frac{1}{\sqrt{4\pi\tau}} e^{-\frac{u^2}{4\tau}}. \quad (\text{D4})$$

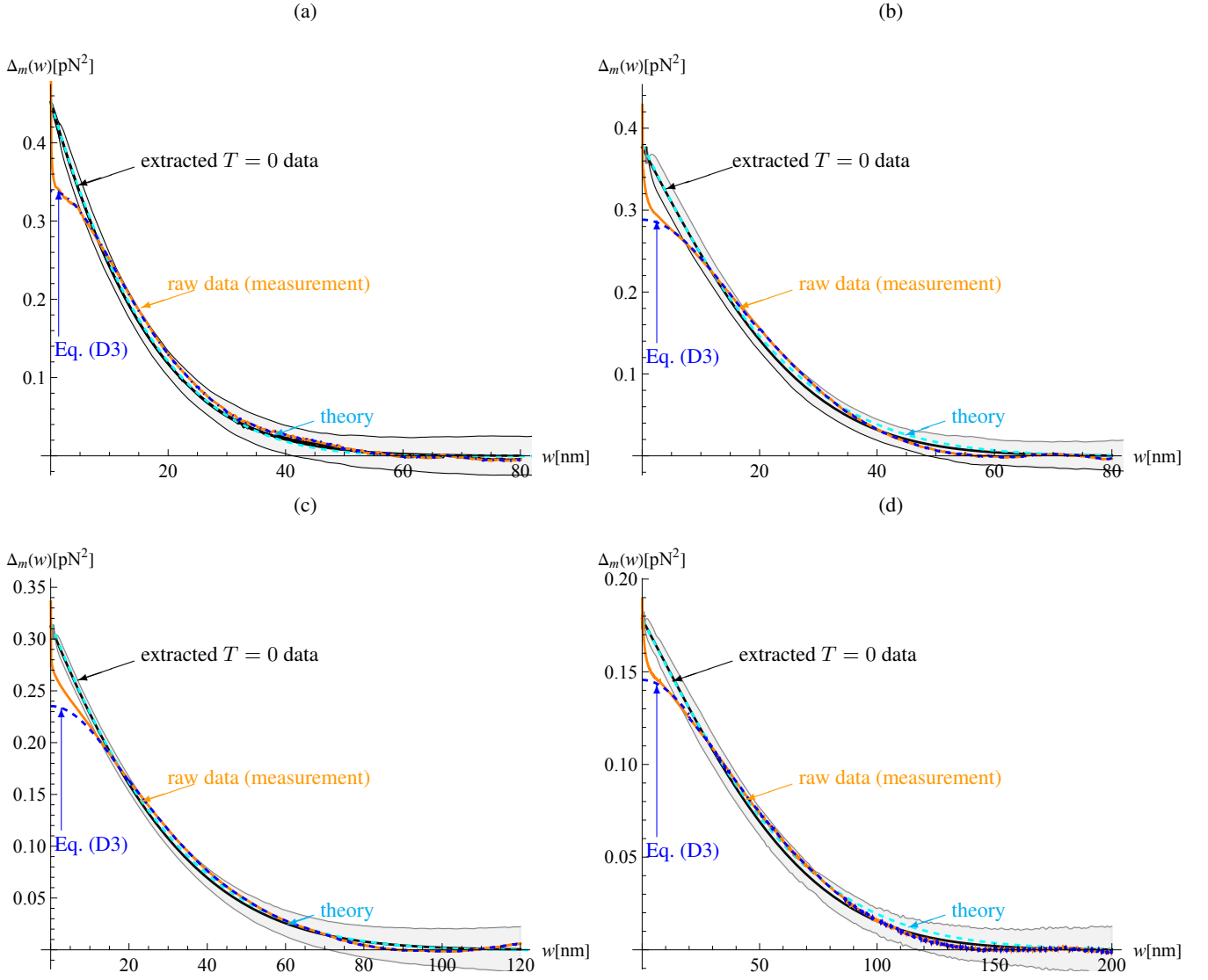


FIG. 8. Comparison of the force correlation  $\Delta_m(w)$  for segments 1-4 in (a-d) extracted at  $T = 0$  (black with grey error bar) with the theoretical prediction (cyan dashed line). The blue line shows the result of (D3), testing our convolution and reconstructing the finite- $T$  data using the diffusion kernel which well reproduces the experimental data (orange). One sees that as  $m^2$  decreases, the correlation length increases and the size of the thermal peak decreases [26].

A nice property of the convolution prescription in Eq. (D4) is that by construction it is area preserving. What remains to be done is to fix the “diffusion time”  $\tau$ . Given the properties of the diffusion kernel, this can analytically be done for

$$\Delta_m(w) = \mathcal{C}e^{-aw-bw^2}. \quad (\text{D5})$$

Demanding that  $\Delta''_{m,T}(0)/\Delta_{m,T}(0)$  agree yields

$$\tau = \frac{t^2}{\pi} - \frac{2a(\pi-2)t^3}{\pi^2} + \mathcal{O}(t^4). \quad (\text{D6})$$

The leading-order term only depends on  $t$ , while the subleading term contains  $a = -\Delta'(0^+)/\Delta(0) \sim 1/\rho_m$ . In the example of Figs. 3(a)–(b) we find  $\tau = 18.87$  at leading order, and  $\tau = 22$  at subleading order. The latter value yields an excellent agreement between approximations (D3) and (D4), and is used in the tests on Fig. 8.